Nonlinear geometric scaling of coercivity in a three-dimensional nanoscale analog of spin ice

I. S. Shishkin,[1] A. A. Mistonov,[1,2] I. S. Dubitskiy,[1] N. A. Grigoryeva,[2] D. Menzel,[3] and S. V. Grigoriev[1,2]
[1]*Petersburg Nuclear Physics Institute, RNC "Kurchatov Institute", Gatchina, 188300 Saint Petersburg, Russia*
[2]*Saint Petersburg State University, 199034 Saint Petersburg, Russia*
[3]*Institut für Physik der Kondensierten Materie, Technische Universität Braunschweig, 38106 Braunschweig, Germany*
(Received 17 September 2015; revised manuscript received 17 June 2016; published 23 August 2016)

Magnetization hysteresis loops of a three-dimensional nanoscale analog of spin ice based on the nickel inverse opal-like structure (IOLS) have been studied at room temperature. The samples are produced by filling nickel into the voids of artificial opal-like films. The spin ice behavior is induced by tetrahedral elements within the IOLS, which have the same arrangement of magnetic moments as a spin ice. The thickness of the films vary from a two-dimensional, i.e., single-layered, antidot array to a three-dimensional, i.e., multilayered, structure. The coercive force, the saturation, and the irreversibility field have been measured in dependence of the thickness of the IOLS for in-plane and out-of-plane applied fields. The irreversibility and saturation fields change abruptly from the antidot array to the three-dimensional IOLS and remain constant upon further increase of the number of layers n. The coercive force H_c seems to increase logarithmically with increasing n as $H_c = H_{c0} + \alpha \ln(n+1)$. The logarithmic law implies the avalanchelike remagnetization of anisotropic structural elements connecting tetrahedral and cubic nodes in the IOLS. We conclude that the "ice rule" is the base of mechanism regulating this process.

DOI: 10.1103/PhysRevB.94.064424

I. INTRODUCTION

Investigations of a new class of geometrically frustrated magnets, called "spin ice" [1–3] started two decades ago and are still in progress. These systems crystallize in the pyrochlore lattice structure consisting of corner-shared tetrahedra with magnetic rare-earth ions at their vertices. The ions possess an Ising-like magnetic moment aligned along the ⟨111⟩ axes of the structure pointing along the tetrahedra's heights. The ground state of this system fulfills the so-called "ice rule," which means that for every tetrahedral cell two magnetic moments are directed into the cell and the two others point out of it. This spin-ice-like moment arrangement leads to interesting properties in the residual entropy [2], the appearance of magnetic quasimonopoles and "magnetricity" [4–6], as well as other intriguing phenomena. At present many attempts are being made to find or to artificially synthesize new examples of such structures [7,8].

Many more experiments are aimed to create nanoscale analogs of spin-ice systems [9–11] in order to obtain new fascinating properties related to geometrical frustration at room temperature. Arrays of single domain nanoislands [9,12] as well as continuous ferromagnetic networks [13,14] are of permanent interest. However, realizations of artificial spin ice (ASI) are mostly two dimensional, and even out-of-plane structures [15] do not totally mimic the original spin-ice structure, which is basically three dimensional. On the other hand, ASI presented in so many variations has already created its own field of study with new physics. The magnetic structure of the ASI can be easily probed by magnetic force microscopy (MFM), while its theoretical description is often based on the results of 2D micromagnetic [13,16,17] or Monte Carlo simulations [18–20]. Owing to these well-developed methods and amazing physical properties the investigation of the artificial spin ice has increased in interest in recent years.

In this paper we study ferromagnetic inverse opal-like structures (IOLS), which can be considered as a first three-dimensional nanoscale analog of the spin-ice system and include at the same time the features of ASI physics. Its three-dimensional structure, however, prevents a direct imaging of a complicated distribution of magnetization inside the IOLS. Neutron diffraction is a common method to resolve the magnetic structure of materials, but the long period of the IOLS forces one to apply small-angle neutron scattering [21–23]. For the interpretation of the results of the SANS experiments we have suggested modeling the remagnetization process in IOLS by using the analog of the "ice rule" [23].

It was shown that the magnetic system of the IOLS consists of Ising-like magnetization vectors directed along the ⟨111⟩ axes and localized in the "legs" connecting the cubes and tetrahedra constituting the IOLS. The "ice rule" defines the number of magnetization vectors pointing in and out of each tetrahedron to be equal. This leads to the fact that the remagnetization process in the IOLS is besides the coercive force characterized by additional critical fields, which have been determined experimentally [23]. Within this micromagnetic model it has recently been shown that the "ice rule" is fulfilled in the tetrahedra of the IOLS in a broad field range [24].

Unfortunately, due to the integrative character of magnetization measurements in terms of the superconducting quantum interference device (SQUID) method and twinning of the IOLS under study [21], it is impossible to observe abrupt changes in the magnetic hysteresis loop similar to those described in Ref. [23]. Nevertheless, in contrast to neutrons the SQUID allows us to study thin film samples and to obtain remagnetization curves for different thicknesses and orientations in quite a short time. Among others, it provides reliable information about the coercive force H_c, the irreversibility field H_{ir}, and the saturation field H_s of the system. In this paper we analyze the values of these fields depending on the thickness and the orientation of the IOLS films with respect to the external magnetic field. Besides that,

 ©2016 American Physical Society

we compare the IOLS characteristics with those of a solid Ni film with the thickness of 3.2 μm.

A typical example of the magnetic properties of an electrodeposited nanocrystalline nickel film can be found in Ref. [25]. It is shown that the magnetization reversal occurs through noncoherent rotation of the magnetization for an in-plane applied magnetic field. The coercive force H_c decreases monotonically with rising film thickness in the range from 10 to 60 μm.

The magnetic properties of the IOLS films have been studied both for cobalt and nickel [26–32]. The nanostructure significantly affects the shape of magnetization loops and drastically changes the coercive field H_c which in the range of 20–1000 nm shows a maximum at a sphere diameter of about 100 nm [27]. As to the large-period structures (larger than 100 nm) it is found that the coercive field is inversely proportional to the diameter of the pores [32]. A similar conclusion was made regarding the coercive field of the magnetic thin film antidot arrays [33]. Measurements of H_c in the magnetic films demonstrated an oscillatory dependence on the film thickness in the range from 0.3 to 3 layers of spheres at least for the $Fe_{50}Ni_{50}$ and Co electrodeposited compounds [28–30], while for pure Ni such oscillations were not observed [31]. On the other hand, as far as we know, there are no such studies present for thick samples, which can be considered as really three-dimensional structures. In addition, orientation dependent properties of IOLS in an external magnetic field have not yet been investigated.

In this paper we demonstrate that the coercive force H_c increases logarithmically with rising thickness of the IOLS. We conclude that it is due to an ASI-like arrangement of the local magnetizations in the "legs" giving rise to an avalanchelike remagnetizing process. We also observe an abrupt change of the irreversibility and saturation fields from the antidot array to the three-dimensional IOLS without any further change upon increase of the sample thickness. We have obtained the coercivity as a function of the angle between the IOLS and the external magnetic field. As a result, we suggest describing the experimental data by a model created for the anisotropic system.

The paper is organized in the following way: In Sec. II we describe the sample preparation procedure and the results of the structural characterization. Section III illustrates the SQUID-magnetometry experiments and the details of data treatment. In Sec. IV experimental results and discussion are presented. Section V gives short concluding remarks.

II. SAMPLES

An inverse opal-like Ni film has been prepared by using a templating technique as reported in Refs. [26,34–36]. A conductive substrate (polished Si single crystal covered by a 20 nm Au layer) was put into an aqueous suspension of polystyrene spheres with a mean diameter of 540 nm at 60 °C [37]. During this vertical deposition method the spheres have arranged in a close-packed colloidal crystal covering an area of 1–2 cm^2 with a thickness larger than 15 μm.

Afterwards, the voids between the spheres were filled with nickel by an electrochemical crystallization process in a three-electrode cell at room temperature. The quantity of the deposited material and, hence, the thickness of the film was controlled by a chronoamperogram experiment. Later on, the thickness of the samples was confirmed by scanning electron microscopy (SEM). In this way samples with a thickness from 0.25 to 14 μm have been produced. Finally, the microspheres were dissolved in toluene for three hours. In addition, a solid nickel film with a thickness of 3.2 μm has been produced using the same electrochemical deposition technique.

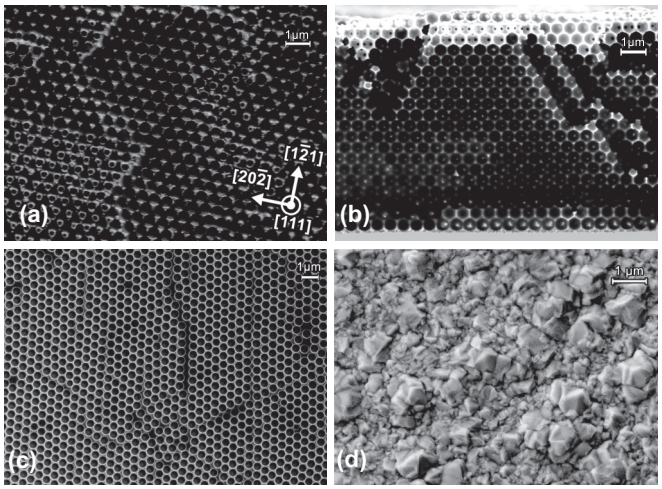

FIG. 1. Top (a) and side (b) views of the Ni_{26} IOLS sample and images of the surface of $Ni_{0.5}$ (c) and Ni_{film} (d).

The SEM images of the samples show the top and side views of an IOLS with a thickness of 13 μm [Figs. 1(a) and 1(b), respectively]. The surface of the IOLS present a well-ordered close-packed array of spherical voids with a lattice constant of about 540 nm. The average lateral size of a structural domain is about 100 μm. Figure 1(c) shows an image of the sample with a thickness of 0.25 μm, which is actually a two-dimensional (2D) hexagonal antidot array. For comparison the surface of the 3.2 μm solid nickel film has also been measured [Fig. 1(d)].

In the following the thickness of the samples will be denoted as the number n of close-packed layers filled with the metal and is indicated as an index in the sample notion Ni_n ($n = 0.5$, 3.5, 8, 17, 26 layers). The solid nickel film is denoted as Ni_{film}.

The microradian x-ray diffraction experiments have shown that the samples with $n > 3$ possess the face-centered cubic (fcc) symmetry with a periodicity of 760 ± 10 nm [22]. The distance between two neighboring sphere centers is 2% smaller than the sphere diameter indicating a sintering of these spheres. As a consequence the volume fraction k of the ferromagnetic material in the IOLS is actually smaller than the volume fraction of the voids for an ideal close-packed structure.

The way of synthesis allows one to attribute the direction perpendicular to the sample substrate to the [111] axis of the fcc structure and the direction of drying of the aqueous suspension (or meniscus moving) to the [20$\bar{2}$] axis. Thus, the orientation of the opal-like crystal is well defined already in the stage of synthesis. These axes are denoted in Fig. 1(a).

Taking the fcc symmetry of the IOLS into account one can figure out the shape of its structural elements (Fig. 2). The latter consists of three parts: a quasitetrahedron, a quasicube, and another quasitetrahedron. They are connected to each

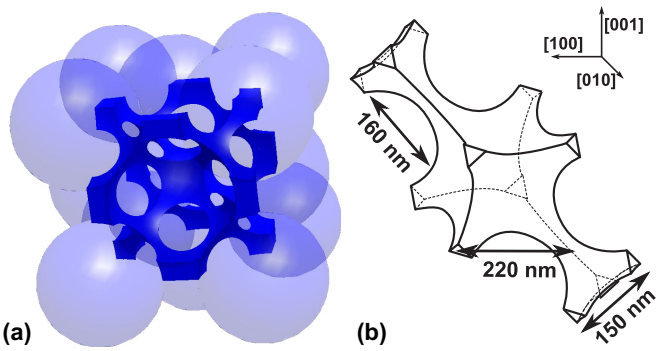

FIG. 2. Unit cell of the IOLS surrounded by the spheres of the initial opal template (a) and basic element of the IOLS (b).

other by vertices (or "legs") aligned along one of the four ⟨111⟩ directions. The surfaces of the cubes and tetrahedra are concave resembling the voids between the spheres. For the IOLS with a period of 760 nm the length of the cube edges are estimated as about 220 nm, while the tetrahedra edges are of the order of 150 nm. The length of the connecting "legs" is approximately 160 nm. Thus, one can conclude that IOLS samples are characterized by the anisotropy due to the specific ⟨111⟩-type directions (structural anisotropy of IOLS) and the film geometry.

III. EXPERIMENT AND DATA REDUCTION

The magnetization reversal process has been studied using a *Quantum Design* MPMS-5S SQUID magnetometer. The magnetic field loops ($-5\,\mathrm{T} \rightarrow 5\,\mathrm{T} \rightarrow -5\,\mathrm{T}$) were performed at $T = 300$ K with the magnetic field applied at different angles θ with respect to the normal of the sample plane [Fig. 3]. The sample was rotated in steps of 5° around the $[20\bar{2}]$ axis of the IOLS, so that the field is perpendicular to the film plane for $\theta = 0^\circ$ ($H \parallel [111]$) and in the sample plane for $\theta = 90^\circ$ ($H \parallel [1\bar{2}1]$).

The hysteresis loops for the Ni_{26} IOLS taken for different orientations are presented in Fig. 4(a). The absolute value of magnetization was not able to be determined within an acceptable accuracy due to the nontrivial shape of the film on the massive substrate. Therefore, we normalized the data set such that the saturation magnetization is assumed to be equal to the bulk value ($M_s = 485$ G) of nickel [38].

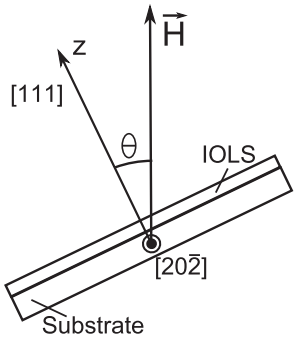

FIG. 3. Geometry of the experiment with the directions of the magnetic field **H** and [111], $[20\bar{2}]$ axes.

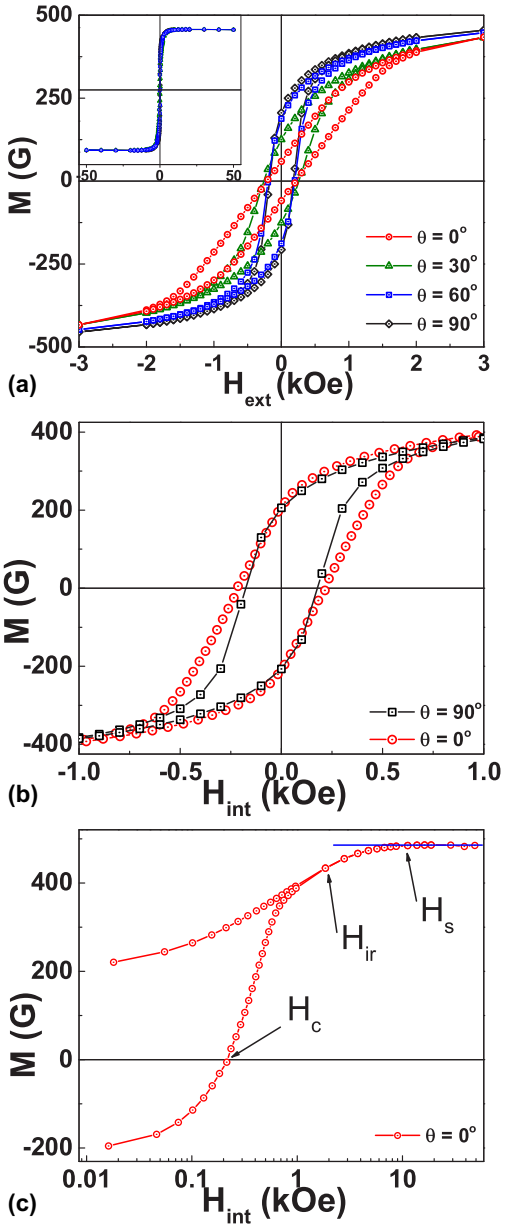

FIG. 4. Magnetization reversal curves for Ni_{26} IOLS for different angles θ plotted as a function of the external (a) and the internal (b) magnetic field. Critical fields derived from the remagnetization curve for $\theta = 0^\circ$ (c).

The evolution of the loops for increasing θ indicates that the film displays strong easy-plane anisotropy. Due to this fact, the demagnetization of the sample has to be taken into account. For this purpose we consider our samples as solid films with magnetization multiplied by the volume ratio of the IOLS and solid film with the same thickness. The internal magnetic field is, therefore, calculated using the following expression [39]:

$$H_z^{\mathrm{int}} = H_z^{\mathrm{ext}} - 4\pi k N_z M_z, \tag{1}$$

where H_z^{int} and H_z^{ext} are the z components of the internal and external magnetic fields, respectively. N_z is the z component of the demagnetization factor of the film. The parameter k is the volume fraction of material in the film. Due to sintering

(see Sec. II) k is about 0.217 for the samples with a thickness larger than three layers and about 0.395 for the $Ni_{0.5}$ sample. The demagnetization factor N_z is assumed to be equal to 1 for the magnetic field perpendicular to the film ($\theta = 0^\circ$), and $N_z = 0$ for the field within the film plane ($\theta = 90^\circ$).

In the following we will restrict ourselves to these two extreme field-to-sample orientations. Thus, demagnetization effects occur only for $\theta = 0^\circ$. A detailed description of the features arising upon angle changing is presented in Appendix A.

The magnetization reversal curves at $\theta = 0^\circ$ and $\theta = 90^\circ$ are presented in Fig. 4(b) as a function of the internal field. The difference between these two curves for small fields ($|H| < 1$ kOe) can originate from the above mentioned estimation of k and/or the deviation of N_z from their assumed values 1 and 0. However, the difference is much smaller than for the curves plotted versus the external field [Fig. 4(a)], and we assume that the easy-plane anisotropy of the film can be neglected in this consideration.

We can distinguish three fields in order to characterize the hysteresis loops as shown in Fig. 4(c). The coercive field (H_c) is the field where the magnetization changes the sign and crosses the field axis. At the irreversibility field (H_{ir}) the upward and downward branches of the loop converge and the hysteresis disappears. The saturation field (H_s) is the smallest field which corresponds to a constant magnetization at high fields. In contrast to the data obtained by small angle neutron diffraction [23], a feature at the field H_{c_1} could not be determined from the SQUID magnetometry due to the smoothness of the region, which H_{c_1} should belong to.

IV. RESULTS AND DISCUSSION

Besides the above mentioned demagnetizing effects, two orientations stand out due to the IOLS spatial structure itself. One of them is the [111] axis, which is the growth direction of the crystal. Even if the crystal is twinned, the sample shows a texture, i.e., the orientation of different crystallites with respect to the field must be the same. Thus, the [111] axis is more specific than the other ⟨111⟩ axes, which to a large extent are averaged over the sample. The second axis, which can be distinguished in a similar way, is the $[1\bar{2}1]$ axis, which is oriented in the plane of the samples. The field applied along this direction should induce a transverse magnetic moment with respect to the field axis [23]. For the SQUID magnetometry with its integrative character these two orientations are very informative, whereas for the others the information of the anisotropy of the IOLS remains hidden.

The three characteristic fields H_c, H_{ir}, and H_s for these two specific orientations are presented in Fig. 5 as a function of the thickness of the IOLS. The difference of about 50 Oe between the values of H_c for $\theta = 0^\circ$ and 90° is significant and can be ascribed to two different origins: The first and most obvious origin is the film anisotropy. As soon as the change of the sample thickness does not affect the film geometry with its easy-plane anisotropy, H_c for $\theta = 0^\circ$ should be larger than for $\theta = 90^\circ$ for a given material.

The second origin is more subtle and can be ascribed to the interplay between the field and the ice rule. However, the energy scale of the ice rule is independent of the orientation of the applied field and, therefore, its contribution should not be so different in the two above mentioned geometries. This holds especially for the 2D structure of the $Ni_{0.5}$ sample, where the ice-rule concept is not applicable.

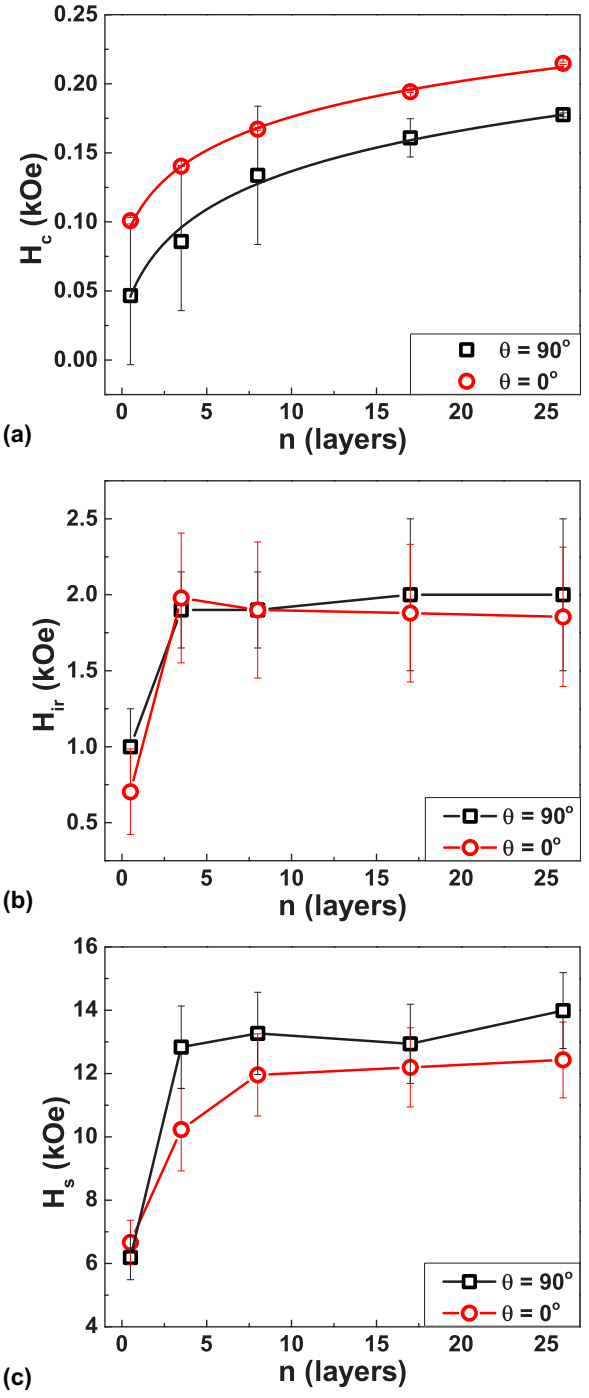

FIG. 5. Thickness dependencies of (a) H_c, (b) H_{ir}, and (c) H_s for the nickel based IOLS.

The ice rule can play a role when the coercive field changes upon transition from the 2D structure to the 3D structure within the same thickness dependences. The further increase of H_c supports only this assumption, and the shape of its change can show its unusual nature. Such an increase was already observed in thinner Ni-based IOLS for $\theta = 90^\circ$ [31].

The H_c-vs-n dependence can be fitted using expression $H_c = H_{c0} + \alpha \ln(n+1)$ [Fig. 5(a)], where $H_{c0} = 80 \pm 2$ Oe and $\alpha = 40 \pm 1$ Oe for $\theta = 0^\circ$, while for $\theta = 90^\circ$, $H_{c0} = 27 \pm 7$ Oe and $\alpha = 45 \pm 2$ Oe.

It is worth noting that the coercive field H_c increases with the thickness for the two extreme field geometries as well as for all other orientations (see Fig. 6). This increase of the coercive field is certainly related to the growth of magnetic domains, or, accounting for the IOLS spatial geometry, the correlated magnetic volume. As mentioned above, the "ice rule" is fulfilled in the tetrahedra of the IOLS in a large field range including fields close to the coercivity [24]. We suppose that the number of correlated "tetrahedra" increase with the sample thickness. Therefore, the field necessary to reorient such an increasing volume should also increase.

If one relates the coercive field H_c to the correlated magnetic volume (for the IOLS film), then the character of the change of H_c is of great importance. Thus, if H_c is increased with the sample thickness as n^α, then all characteristic fields should be correlated to the increase of the number of elements, and long-range order takes place. Opposite to it, if H_c is increased up to a certain value and then saturates, then the correlation volume is limited and short range order, if any at all, occurs as in the case when the correlation length is equal to the element size. The very specific case arises when H_c scales with the sample thickness as $ln(n)$, which means that neither of the two cases will ever be reached. This scaling law can be interpreted as the appearance of large-scale clusters of the unit cell elements based on the ice rule fulfilled in the IOLS.

The literature review given in the Introduction shows that the coercivity does not depend logarithmically on the system size as usual. It is the ASI physics that affects the coercivity by making it a specific point and gives rise to its unusual behavior. The external magnetic field is weak at $H = H_c$ and the arrangement of the local magnetization is regulated by the ice rule only. Its domination provides an increase of the correlated volume and eventually generates the logarithmic dependence of the coercivity on the IOLS thickness.

An example of such behavior was observed by Shen *et al.* in Ref. [16] for the honeycomb artificial spin ice. The remagnetization process in such systems is governed by the avalanchelike mechanism, while the statistics of avalanche lengths depends logarithmically on the system size. In analogy to Ref. [16] we suggested that the magnetization process in the IOLS is probably driven by the similar avalanchelike process for the remagnetization of the "legs." Thus, one can suppose that the logarithmic dependence is the specific feature of artificial spin ice structures realizing the avalanchelike remagnetization mechanism. This hypothesis requires additional experimental and theoretical studies, including and probably focusing on the micromagnetic simulations.

The fields H_{ir} and H_s taken on the scale of the internal field H_{int} practically coincide within the error bars for the field applied at $\theta = 0^\circ$ and 90° [Fig. 5(b) and Fig. 5(c)], respectively. Both fields H_{ir} and H_s do not change with the thickness for $n > 3$ but differ significantly from the values for $n = 0.5$. This drastic change (by a factor of 2–3) originates from the fact that the $Ni_{0.5}$ sample is of 2D and the others are of 3D geometry. In fact, the three layers in the $Ni_{3.5}$ sample are sufficient to form at least one unit cell of the fcc structure of the IOLS with its specific directions. In addition to the conventional crystalline and film anisotropy, the 3D opal-like geometry generates a strong anisotropy due to the IOLS "legs," which are oriented at different angles with respect to the field direction. Even the "simplest" IOLS formed by three layers requires a higher field (i) to make the loop reversible (H_{ir}) and (ii) to saturate the sample (H_s). Since H_{ir} and H_s do not change with increasing number of layers n, one can conclude that the field interacts independently with each basic element of the structure at fields $H \gtrsim H_{ir}$. In other words, for larger fields the local magnetization direction inside each "leg" follows coherently the external field. In contrast, for small magnetic fields the interaction between neighboring local magnetic elements of the IOLS dominates the field, which results in the observed thickness dependence of the coercive field H_c.

V. CONCLUDING REMARKS

Ferromagnetic Ni-based inverted opal-like structures have been considered as an example of a three-dimensional nanoanalog of spin ice and were studied by SQUID magnetometry at room temperature. The three fields H_c, H_{ir}, and H_s, which are characteristic for the magnetization reversal process, were studied as a function of the film thickness and the sample-to-field orientation.

The existence of the complicated spatial structure as in IOLS leads to an increase of the coercivity H_c as compared to the solid film. The coercivity rises monotonically with the thickness of the sample following a logarithmic law, which can be attributed to an avalanchelike remagnetization process of the "legs" within the IOLS. This process is connected to the increase of the energy needed to reorient the magnetic subsystems of the IOLS. The difference of H_c for two geometries remains constant over the full thickness range, which results from the film easy-plane anisotropy. The spatial structure of the IOLS influences only the field range close to or smaller than the coercive field, whereas it affects neither H_{ir} nor H_s. The values of H_{ir} and H_s change abruptly upon change from a 2D hexagonal antidot array to the 3D IOLS.

The observed orientation dependence of the coercive field demonstrates a coherent and an incoherent mechanism of the remagnetization and describes (i) the rotation of the magnetization vectors under the influence of the field component perpendicular to the easy axis and (ii) the effect of the demagnetizing field of the specimen. We conclude that the magnetization reversal process for the coherent mechanism takes place by sequential pinning of the magnetization along the $\langle 111 \rangle$-type axes.

ACKNOWLEDGMENTS

The authors acknowledge the help of N. A. Sapoletova, K. S. Napolskii, and A. A. Eliseev from the Department of Materials Science of the Moscow State University for samples synthesis. We thank our collegue G. A. Valkovskiy from the Saint-Petersburg State University for fruitful discussions. We are indebted to the Interdisciplinary Center for Nanotechnology at the Research Park of the St. Petersburg State University for the SEM investigations. The authors also thank the Saint-Petersburg State University for the research Grant

No. 11.42.1311.2014. The work is supported by the German Academic Exchange Service (DAAD) in the framework of the "Mikhail Lomonosov II" and the G-RISC program and by the Russian Foundation for Basic Research (Project No. 14-22-01113).

APPENDIX: ORIENTATION DEPENDENCE

The orientation dependence of the coercive field H_c for samples with different thicknesses is presented in Fig. 6. The different principal axes of the IOLS which correspond to the angles θ with respect to the normal of the sample plane are indicated on the top of the graph.

When the field is oriented along one of these axes, one would expect that this symmetric configuration would lead to pronounced features in the coercivity. However, such features are not observed in the experimental data [Fig. 6]. The reason is most likely connected to a twinning of the crystal [22]. When the field direction coincides with the principal axis of one twin, it does not for the other twin at the same time. For instance, a symmetrical configuration arises for one twin at 0, 19, and 55 degrees, whereas it occurs for another one at 0, 35, and 71 degrees (indicated by different colors in Fig. 6). As a result, the magnetization of the twins both contribute to the measurement and are, therefore, mixed in any direction.

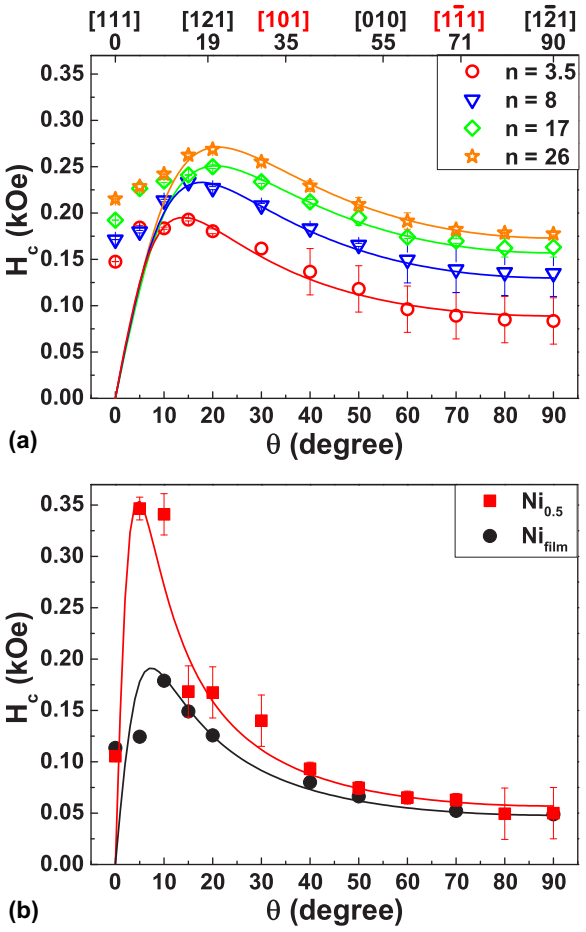

FIG. 6. Angular dependence of the coercivity H_c for a Ni-based IOLS with different thicknesses (a). The main crystallographic axes of IOLS corresponding to the field orientation are shown on the top of the graph. Angular dependence of the coercivity H_c for $Ni_{0.5}$ and the Ni film (b).

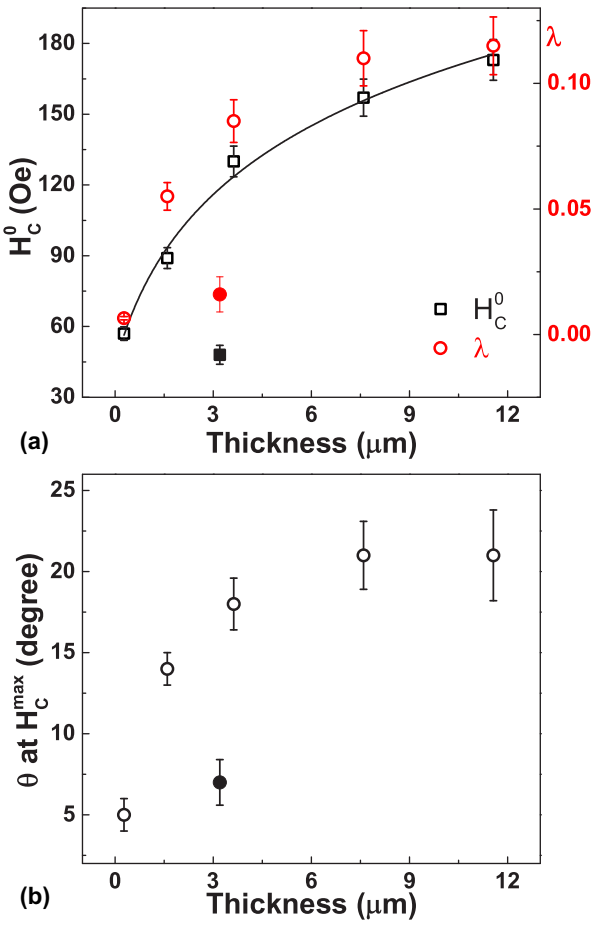

FIG. 7. Thickness dependence of the orientation dependent fit parameters H_c^0 and λ for Ni-based IOLS (empty symbols) and for the film (solid symbols). The solid line shows the fit by the logarithmic function (a). Thickness dependence of the critical angle corresponding to the maximum coercive field for Ni IOLS (empty symbols) and for the film (solid symbols) (b).

Nevertheless, it is obvious that H_c depends nonmonotonically on the field-to-sample orientation. All curves in Fig. 6 show an increase of H_c with the angle starting from $\theta = 0°$ to a critical angle θ_c and a smooth decrease of H_c from θ_c to $\theta = 90°$. Our data confirm previous observations on nickel-based OLS [26].

The region below the critical angle θ_c corresponds to the coherent rotation of the magnetization [40,41], whereas the region above the critical angle θ_c belongs to the incoherent regime. The latter comprises different reversal modes like "curling," fanning, "vortex," and reverse by a combination of quasicoherent "flower" and "vortex" [42–45]. Based on a theoretical and micromagnetic model [44,45] the incoherent reversal modes can be observed in the samples containing magnetic particles which are (i) uniform in size and shape, (ii) uniformly spaced, and (iii) mutually aligned. Despite that the IOLS films fit well the description above, their spatial structure is more complicated than simple chains or arrays [46–49] of

identical nanoparticles. Therefore, incoherent reversal modes are not expected to give a satisfactory description of the experimental results.

However, IOLS samples show a well pronounced magnetic anisotropy. Thus, a fit of the experimental angle dependency of H_c was performed as described in Ref. [50] for magnetically anisotropic ferromagnetic crystals ([Fig. 6], solid curves). The calculation takes into account (i) the rotation of the magnetization vectors under the influence of field component perpendicular to the easy axis of magnetization and (ii) the effect of the demagnetizing fields of the specimen. In this case the angular dependence of H_c can be described by the following expression:

$$H_c = \frac{H_c^0 \sin\theta}{\lambda\cos^2\theta + \sin^2\theta}, \quad \lambda = \frac{N_z M_s}{H_A + N_y M_s}, \tag{A1}$$

where N_y and N_z denote the effective demagnetizing factors of the film specimen, $H_A = 2K/M_s$ the anisotropy field, and K the magnetocrystalline anisotropy constant of the ferromagnet.

In the incoherent regime the angle dependence is well described by Eq. (A1), while the decrease of $H_c(\theta)$ below the critical angle is much more pronounced for the theoretical curves in comparison to the experimental data (Fig. 6). In addition, the value of H_c for $\theta = 0^\circ$ is close to zero for the theoretical curves, whereas it is comparable to the H_c at $\theta = 90^\circ$ in the experiment. This may be due to the fact that four easy axes of magnetization are present in the IOLS sample instead of only one as in the used model [50]. One of the easy axes is aligned perpendicular to the film. The three other axes are oriented at an angle of 19 degrees with respect to the film. Thus, the magnetization reversal process takes place by a sequential pinning of the magnetization along the ⟨111⟩-type axes at angles lower than θ_c. Furthermore, the configuration of the demagnetizing fields is supposed to be more complicated than for an ordinary film. We also have to note that the procedure of magnetization reversal measurements described in Ref. [50], where the initial magnetization process was carried out always along the easy axis, is different from our experiment.

A similar orientation dependence of H_c is observed for the solid Ni film (Fig. 6). The formation of polycrystalline films with well-formed grains [Fig. 1(d)] leads to an increased domain wall pinning at grain boundaries, which is assumably most efficient when the walls are parallel to the boundaries. If the orientation of the grain boundaries is distributed such that they are aligned on a cone with a quite definite angle with respect to the substrate normal, a maximum of H_c is expected to appear at that angle [51,52].

The coercive field H_c for the solid film is smaller than for any of the IOLS (Fig. 6). The orientation dependence of H_c of the sample with $n = 0.5$ is very close to that for the solid nickel film in a wide angle range and differs from the other IOLS samples, which is a fingerprint of the two-dimensional nature of this antidot array.

H_c^0 extracted from the orientation dependence follows a logarithmic law with the thickness in the same way as the experimental H_c [Fig. 7(a)], while λ and θ_c do not change upon an increasing film thickness beyond 17 layers [Fig. 7(b)]. This means that the demagnetizing field appearing due to the film anisotropy becomes decisive for samples with $n > 17$.

The similarity of the orientation dependence of the systems with different structural dimensionality (and even in the solid film) is most likely caused by the common film-like geometry. Hence, the orientation dependence of H_c cannot be used for the study of the magnetic properties of the IOLS, which, in our opinion, is governed to a large extent by the "ice rule" concept.

[1] M. J. Harris, S. T. Bramwell, D. F. McMorrow, T. Zeiske, and K. W. Godfrey, Phys. Rev. Lett. **79**, 2554 (1997).

[2] A. P. Ramirez, A. Hayashi, R. J. Cava, R. Siddharthan, and B. S. Shastry, Nature (London) **399**, 333 (1999).

[3] M. J. P. Gingras, *Introduction to Frustrated Magnetism* (Springer, Berlin, Heidelberg, 2011), Vol. 164, p. 293.

[4] C. Castelnovo, R. Moessner, and S. L. Sondhi, Nature (London) **451**, 42 (2008).

[5] L. Bovo, J. A. Bloxsom, D. Prabhakaran, G. Aeppli, and S. T. Bramwell, Nat. Commun. **4**, 1535 (2013).

[6] S. J. Blundell, Phys. Rev. Lett. **108**, 147601 (2012).

[7] L.-J. Chang, S. Onoda, Y. Su, Y.-J. Kao, K.-D. Tsuei, Y. Yasui, K. Kakurai, and M. R. Lees, Nat. Commun. **3**, 992 (2012).

[8] A. M. Hallas, A. M. Arevalo-Lopez, A. Z. Sharma, T. Munsie, J. P. Attfield, C. R. Wiebe, and G. M. Luke, Phys. Rev. B **91**, 104417 (2015).

[9] R. F. Wang, C. Nisoli, R. S. Freitas, J. Li, W. McConville, B. J. Cooley, M. S. Lund, N. Samarth, C. Leighton, V. H. Crespi, and P. Schiffer, Nature (London) **439**, 303 (2006).

[10] R. V. Chopdekar, G. Duff, R. V. Hügli, E. Mengotti, D. A. Zanin, L. J. Heyderman, and H. B. Braun, New J. Phys. **15**, 125033 (2013).

[11] W. R. Branford, S. Ladak, D. E. Read, K. Zeissler, and L. F. Cohen, Science **335**, 1597 (2012).

[12] E. Mengotti, L. J. Heyderman, A. F. Rodríguez, F. Nolting, R. V. Hügli, and H.-B. Braun, Nat. Phys. **7**, 68 (2011).

[13] K. Zeissler, S. K. Walton, S. Ladak, D. E. Read, T. Tyliszczak, L. F. Cohen, and W. R. Branford, Sci. Rep. **3**, 1252 (2013).

[14] M. Tanaka, E. Saitoh, H. Miyajima, T. Yamaoka, and Y. Iye, Phys. Rev. B **73**, 052411 (2006).

[15] S. Zhang, J. Li, I. Gilbert, J. Bartell, M. J. Erickson, Y. Pan, P. E. Lammert, C. Nisoli, K. K. Kohli, R. Misra, V. H. Crespi, N. Samarth, C. Leighton, and P. Schiffer, Phys. Rev. Lett. **109**, 087201 (2012).

[16] Y. Shen, O. Petrova, P. Mellado, S. Daunheimer, J. Cumings, and O. Tchernyshyov, New J. Phys. **14**, 035022 (2012).

[17] C. I. L. de Araujo, R. C. Silva, I. R. B. Ribeiro, F. S. Nascimento, J. F. Felix, S. O. Ferreira, L. A. S. Mó, W. A. Moura-Melo, and A. R. Pereira, Appl. Phys. Lett. **104**, 092402 (2014).

[18] G.-W. Chern, M. J. Morrison, and C. Nisoli, Phys. Rev. Lett. **111**, 177201 (2013).

[19] J. Drisko, S. Daunheimer, and J. Cumings, Phys. Rev. B **91**, 224406 (2015).

[20] I. Gilbert, G.-W. Chern, S. Zhang, L. O'Brien, B. Fore, C. Nisoli, and P. Schiffer, Nat. Phys. **10**, 670 (2014).

[21] S. V. Grigoriev, K. S. Napolskii, N. A. Grigoryeva, A. V. Vasilieva, A. A. Mistonov, D. Yu. Chernyshov, A. V. Petukhov, D. V. Belov, A. A. Eliseev, A. V. Lukashin, Yu. D. Tretyakov, A. S. Sinitskii, and H. Eckerlebe, Phys. Rev. B **79**, 045123 (2009).

[22] N. A. Grigoryeva, A. A. Mistonov, K. S. Napolskii, N. A. Sapoletova, A. A. Eliseev, W. Bouwman, D. V. Byelov, A. V. Petukhov, D. Yu. Chernyshov, H. Eckerlebe, A. V. Vasilieva, and S. V. Grigoriev, Phys. Rev. B **84**, 064405 (2011).

[23] A. A. Mistonov, N. A. Grigoryeva, A. V. Chumakova, H. Eckerlebe, N. A. Sapoletova, K. S. Napolskii, A. A. Eliseev, D. Menzel, and S. V. Grigoriev, Phys. Rev. B **87**, 220408(R) (2013).

[24] I. S. Dubitskiy, A. V. Syromyatnikov, N. A. Grigoryeva, A. A. Mistonov, and S. V. Grigoriev, arXiv:1509.05201.

[25] E. V. Sukovatitsina, A. S. Samardak, A. V. Ognev, L. A. Chebotkevich, A. Yu. Samardak, M. R. Sanaeian, F. Nasirpouri, Solid State Phenomena **215**, 139 (2014).

[26] L. Xu, L. D. Tung, L. Spinu, A. A. Zakhidov, R. H. Baughman, and J. B. Wiley, Adv. Mater. **15**, 1562 (2003).

[27] A. A. Zhukov, M. A. Ghanem, A. V. Goncharov, P. A. J. de Groot, I. S. El-Hallag, P. N. Bartlett, R. Boardman, and H. Fangoh, J. Magn. Magn. Mater. **272-276**, 1621 (2004).

[28] A. A. Zhukov, A. V. Goncharov, P. A. J. de Groot, M. A. Ghanem, I. S. El-Hallag, and P. N. Bartlett, R. Boardman, H. Fangohr, V. Novosad, and G. Karapetrov, J. Appl. Phys. **97**, 10J701 (2005).

[29] A. A. Zhukov, A. V. Goncharov, P. A. J. de Groot, M. A. Ghanem, P. N. Bartlett, R. Boardman, H. Fangohr, V. Novosad, and G. Karapetrov, Appl. Phys. Lett. **88**, 062511 (2006).

[30] P. A. J. de Groot, A. A. Zhukov, R. Boardman, G. Bordignon, H. Fangohr, and P. N. Bartlett, J. Magn. Magn. Mater. **310**, e846 (2007).

[31] Y. Hao, F. Q. Zhu, C. L. Chien, and P. C. Searson, J. Electrochem. Soc. **154**, D65 (2007).

[32] I. S. El-Hallag, Mater. Sci. Poland **28**, 245 (2010).

[33] I. Ruiz-Feal, L. Lopez-Diaz, A. Hirohata, J. Rothman, C. M. Guertler, J. A. C. Bland, L. M. Garcia, J. M. Torres, J. Bartolome, F. Bartolome, M. Natali, D. Decanini, and Y. Chen, J. Magn. Magn. Mater. **242-245**, 597 (2002).

[34] A. A. Grunin, N. A. Sapoletova, K. S. Napolskii, A. A. Eliseev, and A. A. Fedyanin, J. Appl. Phys. **111**, 07A948 (2012).

[35] P. N. Bartlett, P. R. Birkin, and M. A. Ghanem, Chem. Commun. **17**, 1671 (2000).

[36] L. Xu, W. L. Zhou, C. Frommen, R. H. Baughman, A. A. Zakhidov, L. Malkinski, J.-Q. Wang, and J. B. Wiley, Chem. Commun. **12**, 997 (2000).

[37] A. I. Plekhanov, D. V. Kalinin, and V. V. Serdobintseva, Ross. Nanotekh. **1**, 245 (2006) (in Russian).

[38] C. Kittel, *Introduction to Solid State Physics* (Wiley, New York, 1953).

[39] C. Kittel, Phys. Rev. **73**, 155 (1948).

[40] E. C. Stoner and E. P. Wohlfarth, Philos. Trans. R. Soc. London A **240**, 599 (1948).

[41] E. P. Wohlfarth, J. Appl. Phys. Suppl. **30**, S117 (1960).

[42] E. H. Frei, S. Shtrikman, and D. Treves, Phys. Rev. **106**, 446 (1957).

[43] I. S. Jacobs and C. P. Bean, Phys. Rev. **100**, 1060 (1955).

[44] W. Williams and D. J. Dunlop, J. Geophys. Res. **100**, 3859 (1995).

[45] K. Fabian, A. Kirchner, W. Williams, F. Heider, T. Leibl, and A. Hubert, Geophys. J. Int. **124**, 89 (1996).

[46] S. Goolaup, N. Singh, A. O. Adeyeye, V. Ng, and M. B. A. Jalil, Eur. Phys. J. B **44**, 259 (2005).

[47] O. Albrecht, R. Zierold, S. Allende, J. Eschrig, C. Patzig, B. Rauschenbach, K. Nielsch, and D. Gorlitz, J. Appl. Phys. **109**, 093910 (2011).

[48] R. Lavin, J. C. Denardin, A. P. Espejo, A. Cortés, and H. Gómez, J. Appl. Phys. **107**, 09B504 (2010).

[49] L. Sun, P. C. Searson, and C. L. Chien, Appl. Phys. Lett. **79**, 4429 (2001).

[50] Ya. S. Shur, G. S. Kandaurova, and L. G. Onoprienko, J. Exp. Theoret. Phys. **21**, 292 (1965).

[51] M. A. Abdellateef, L. Emke, and C. Heiden, Phys. Status Solidi A **147**, K39 (1995).

[52] M. M. Kulyk, V. M. Kalita, A. F. Lozenko, S. M. Ryabchenko, O. V. Stognei, A. V. Sitnikov, and V. Korenivski, J. Phys. D: Appl. Phys. **47**, 345002 (2014).